

Analytical solution to incident angle quasi-phase-matching engineering for second harmonic generation in a periodic-poled lithium niobate crystal

Li-Hong Hong(洪丽红), Ya-Ting Qiu(邱雅婷), Xiao-Ni Li(李晓霓), Bao-Qin Chen(陈宝琴), and Zhi-Yuan Li(李志远)

Citation: Chin. Phys. B, 2024, 33 (**2**): 020301. DOI: 10.1088/1674-1056/ad0628
Journal homepage: http://cpb.iphy.ac.cn; http://iopscience.iop.org/cpb

What follows is a list of articles you may be interested in

Improved statistical fluctuation analysis for two decoy-states phase-matching quantum key distribution

Jiang-Ping Zhou(周江平), Yuan-Yuan Zhou(周媛媛), Xue-Jun Zhou(周学军), and Xuan Bao(暴轩)
Chin. Phys. B, 2023, 32 (**8**): 080306. DOI: 10.1088/1674-1056/acbdea

Improving source-in-the-middle continuous-variable quantum key distribution using a heralded hybrid linear amplifier

Lei-Xin Wu(伍磊鑫), Yan-Yan Feng(冯艳艳), and Jian Zhou(周健)
Chin. Phys. B, 2023, 32 (**7**): 070310. DOI: 10.1088/1674-1056/ac9b39

Entanglement properties of superconducting qubits coupled to a semi-infinite transmission line

Yang-Qing Guo(郭羊青), Ping-Xing Chen(陈平形), and Jian Li(李剑)
Chin. Phys. B, 2023, 32 (**6**): 060302. DOI: 10.1088/1674-1056/acc0fa

Rigorous solution to second harmonic generation considering transmission and reflection of light at air-crystal interface

Ya-Ting Qiu(邱雅婷), Li-Hong Hong(洪丽红), and Zhi-Yuan Li(李志远)
Chin. Phys. B, 2023, 32 (**5**): 050301. DOI: 10.1088/1674-1056/ac9fc5

Performance analysis of quantum key distribution using polarized coherent-states in free-space channel

Zengte Zheng(郑增特), Ziyang Chen(陈子扬), Luyu Huang(黄露雨),Xiangyu Wang(王翔宇), and Song Yu(喻松)
Chin. Phys. B, 2023, 32 (**3**): 030306. DOI: 10.1088/1674-1056/ac7450

Analytical solution to incident angle quasi-phase-matching engineering for second harmonic generation in a periodic-poled lithium niobate crystal

Li-Hong Hong(洪丽红)[1,2,†], Ya-Ting Qiu(邱雅婷)[2,†], Xiao-Ni Li(李晓霓)[2,†], Bao-Qin Chen(陈宝琴)[2], and Zhi-Yuan Li(李志远)[2,‡]

[1] *State Key Laboratory of High Field Laser Physics, Shanghai Institute of Optics and Fine Mechanics, Chinese Academy of Sciences, Shanghai* 201800, *China*
[2] *School of Physics and Optoelectronics, South China University of Technology, Guangzhou* 510640, *China*

(Received 5 September 2023; revised manuscript received 13 October 2023; accepted manuscript online 24 October 2023)

Phase matching or quasi-phase matching (QPM) is of significant importance to the conversion efficiency of second harmonic generation (SHG) in artificial nonlinear crystals like lithium niobate (LN) crystal or microstructured nonlinear crystals like periodic-poled lithium niobate (PPLN) crystals. In this paper, we propose and show that the incident angle of pump laser light can be harnessed as an alternative versatile tool to engineer QPM for high-efficiency SHG in a PPLN crystal, in addition to conventional means of period adjusting or temperature tuning. A rigorous model is established and analytical solution of the nonlinear conversion efficiency under the small and large signal approximation theory is obtained at different incident angles. The variation of phase mismatching and walk-off length with incident angle or incident wavelength are also explored. Numerical simulations for a PPLN crystal with first order QPM structure are used to confirm our theoretical predictions based on the exact analytical solution of the general large-signal theory. The results show that the narrow-band tunable SHG output covers a range of 532 nm–552.8 nm at the ideal incident angle from 0° to 90°. This theoretical scheme, fully considering the reflection and transmission at the air-crystal interface, would offer an efficient theoretical system to evaluate the nonlinear frequency conversion and help to obtain the maximum SHG conversion efficiency by selecting an optimum incident wavelength and incident angle in a specially designed PPLN crystal, which would be very helpful for the design of tunable narrow-band pulse nanosecond, picosecond, and femtosecond laser devices via PPLN and other microstructured LN crystals.

Keywords: nonlinear frequency conversion, transmission, reflection, lithium niobate

PACS: 03.50.De, 42.70.Mp, 42.25.Bs, 78.20.Ci **DOI:** 10.1088/1674-1056/ad0628

1. Introduction

Laser has a limited wavelength range since it has been invented.[1] Due to the discovery of second-harmonics generation (SHG), the boom of nonlinear optics was opened. The interaction of laser light with diverse nonlinear crystals,[2–6] leading to various nonlinear optical processes such as SHG, sum-frequency generation (SFG), difference-frequency (DFG), and others, offers a powerful and versatile way to generate new optical frequencies and provides a wealth of possibilities to expand the wavelength range of lasers. For the process of SHG, the dispersion of nonlinear media makes the fundamental wave (FW) and the second-harmonic wave (SHW) have different phase velocities in the dielectric material of nonlinear crystal, resulting in a phase-mismatching. To satisfy the phase matching conditions, the birefringence phase matching (BPM)[7,8] and quasi-phase matching (QPM)[9–16] technologies have been explored and become two commonly used technical methods. Compared with the limitations of BPM, QPM is more preferred by virtue of its high nonlinear susceptibility tensor, flexible nonlinear medium selection, as well as various tuning methods, which can compensate phase-mismatching by modulating the sign of nonlinear coefficients. As an attractive nonlinear optical material, lithium niobate (LN) crystal possesses some superior features such as excellent nonlinear optical properties, broad transparency range, and more uniquely, capability to build microstructures with ferroelectric domain inversion that enables QPM.[17,18] Many second-order nonlinear effects[19–25] have been fully developed within the LN nonlinear crystals including periodic poled lithium niobate (PPLN) crystal. Recently, people have realized the specific-wavelength SHG output by the PPLN crystal, and the broad-band SHG output via the chirped periodic poled lithium niobate (CPPLN). It is also worth mentioning that in recent years, with the rapid development of thin film technology on lithium niobate insulators and related surface micro-nano manufacturing technology, lithium niobate has been used to achieve a series of miniaturized, integrated, high-quality, high-performance photonic functional devices.[26–30]

The physical understanding of various nonlinear optical processes in LN crystals involve solution of transport of FW within LN crystal, its excitation of SHW, the transport of SHW, and the mutual interaction and coupling between FW and SHW. The physics is a little bit complicated, and

[†]These authors contributed equally to this work.
[‡]Corresponding author. E-mail: phzyli@scut.edu.cn

© 2024 Chinese Physical Society and IOP Publishing Ltd

the corresponding mathematics is also some certain troublesome, especially when considering that LN crystal and many other nonlinear crystals are anisotropic materials rather than simple isotropic materials. There have existed some schemes that extensively only investigate the reflection and transmission of incident wave from isotropic medium to uniaxial crystal interface,[31–39] such as the classical electromagnetic theoretical analysis method.[37–39] However, the implementation of a specific SHG in PPLN crystal usually utilizes the collinear configuration where the pump FW light and generated SHW light beam is parallel. This geometric configuration has some limitations for expanding the nonlinear frequency conversion range. First, the pump light is normally incident upon the PPLN nonlinear crystals. In this case, QPM for a single wavelength that is designed to match the specific PPLN pitch size of inverted ferroelectric domains can be intelligently achieved, but not for other wavelengths, thus the bandwidth is limited. As far as we know, very rare reports were presented on the generation of narrow-band tunable SHG based on QPM technology via a PPLN crystal.

In this work, we theoretically investigate the non-collinear configuration of SHG via QPM in a PPLN crystal, where the pump light impacts the PPLN crystal surface at different angles, and explore a new way to expand the bandwidth of SHG for a single PPLN crystal via incident angle tuning. We calculate the reflection coefficient and transmission coefficient at air-crystal interface in LN crystal and derive the coupled-wave equations to describe the interaction between FW and SHW non-collinearly transporting in crystal. We analyze the phase mismatching when the light is incident at different angles, study the walk-off effect between the transmission FW and SHW in LN crystal, and investigate the accomplishment of QPM via the angle tuning in a PPLN crystal with first-order QPM structure at different pump laser wavelength. We wish to create a complete theoretical system to quantitatively evaluate the SHG process uncovering the reflection and transmission of pump light at the air-crystal surface across a wide range of incident angles at different incident pump wavelengths, and explore the possibility to realize narrow-band tunable lasers by simply controlling the incident angle in a PPLN crystal working in the framework of QPM technology. Surely, such a study should have an important practical significance in actual experiments and laser architectures.

study should have an important practical significance in actual experiments and laser architectures.

2. Principle of oblique incidence angle tuning for SHG

2.1. Theoretical model establishment and crystal interface analysis

In our physical mode, a z-cut LN crystal is used as the nonlinear medium, and the schematic configuration is shown in Fig. 1(a). The extraordinary crystalline axis of LN sample is along the z axis, while its ordinary crystalline plane is coplanar with the xoy plane. We presume that a beam of TE-polarized pump light with electromagnetic field components (E_z, H_x, H_y) and the wave vector k_i is incident on the LN crystal surface from air at an angle α with y axis, and transports within the xoy plane. Further analysis with the specific illustration of the incident light at the interface of the two media (air and LN crystal) is displayed in Fig. 1(b). As we know, the refractive index n_0, relative dielectric constant $\varepsilon_{\mathrm{r}1}$ and relative permeability $\mu_{\mathrm{r}1}$ of air, the relative permeability μ_1 of crystal are all of values 1. The relative dielectric constant ε_1 in this case is equal to ε_z in crystal for FW. In such a scheme, the pump light transmitted into the LN crystal is extraordinary light, and the refractive index of FW and SHW is defined as n_1 and n_2 respectively. The scheme we adopted guarantees the use of the maximum nonlinear polarization tensor d_{33} (about 27 pm/V) of the crystal, which is the most favorable configuration for driving an efficient nonlinear frequency up-conversion process and corresponds to the extraordinary refractive index surfaces of the crystal ellipsoid. Maximum spatial overlap of field E_{1z} and E_{2z} distributions can be achieved. Therefore,

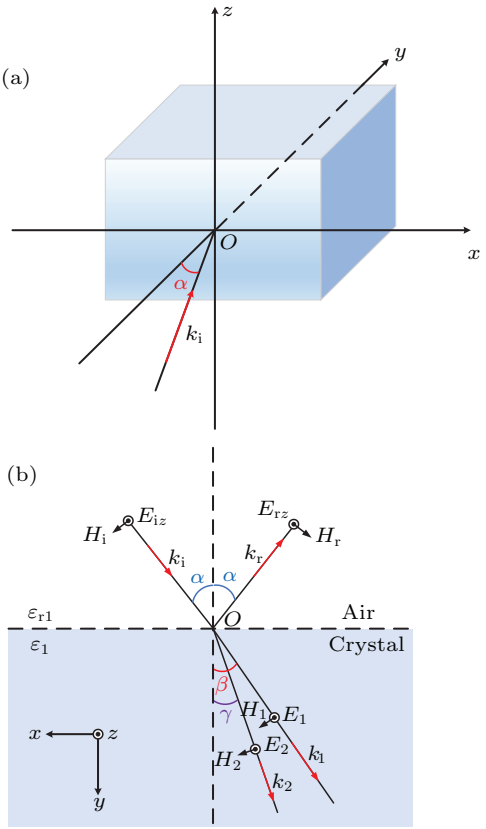


Fig. 1. (a) Schematic configuration of a z-cut LN crystal in the air, a TE-polarized pump light reaches on the crystal surface in xoy plane at an angle α with y axis. (b) The cross-sectional view of the light propagations and electromagnetic field analysis of incident wave, reflection wave, transmission wave (FW), and SHW from air to LN crystal, responding to wave vectors k_i, k_r, k_1 (k_t), k_2, respectively. $\varepsilon_{\mathrm{r}1}$ and ε_1 are the relative dielectric constants of air and crystal for transmission wave (FW). α is incident (also the reflection) angles of FW, β and γ are the transmission angle of FW and SHW, respectively.

the refractive index n_1 of the FW and the refractive index n_2 of the SHG refer to the refractive index of extraordinary light in the LN crystal. The angle of the transmitted FW wave vector k_1 with the y axis is β, and that of SHW vector k_2 with the y axis is γ. Notably, we approximately regard the LN crystal as an infinite crystal, as in most textbooks of nonlinear optics. Considering the transmission and reflection of FW at the LN crystal front (first) surface, the crystal will be a semi-infinite crystal so that the influence from the back (second) surface can be neglected.

Here, the FW and SHW light involved are both electromagnetic waves so that all their physical and chemical properties are dictated by the space–time evolution of electromagnetic field. Therefore, we can conduct our analysis from the following set of Maxwell's equations for a monochromatic incident FW light with angular frequency ω_1, which are

$$\begin{aligned}\nabla\times\boldsymbol{E}&=\mathrm{i}\omega_1\mu_0\mu_\mathrm{r}\boldsymbol{H},\\ \nabla\times\boldsymbol{H}&=-\mathrm{i}\omega_1\varepsilon_0\varepsilon_\mathrm{r}\boldsymbol{E},\end{aligned}\tag{1}$$

where μ_r is relative permeability of the corresponding medium. Subsequently, we suppose that the electric field of incident wave, reflection wave, and transmission wave are expressed as

$$\begin{aligned}E_\mathrm{iz}&=E_\mathrm{i}\,\mathrm{e}^{-\mathrm{i}k_\mathrm{ix}x+\mathrm{i}k_\mathrm{iy}y}\,\mathrm{e}^{-\mathrm{i}\omega_1 t},\\ E_\mathrm{rz}&=E_\mathrm{r}\,\mathrm{e}^{-\mathrm{i}k_\mathrm{rx}x-\mathrm{i}k_\mathrm{ry}y}\,\mathrm{e}^{-\mathrm{i}\omega_1 t},\\ E_\mathrm{tz}&=E_\mathrm{t}\,\mathrm{e}^{-\mathrm{i}k_\mathrm{tx}x+\mathrm{i}k_\mathrm{ty}y}\,\mathrm{e}^{-\mathrm{i}\omega_1 t},\end{aligned}\tag{2}$$

where $k_\mathrm{i}=\sqrt{k_\mathrm{ix}^2+k_\mathrm{iy}^2}$, $k_\mathrm{r}=\sqrt{k_\mathrm{rx}^2+k_\mathrm{ry}^2}$, and $k_\mathrm{t}=\sqrt{k_\mathrm{tx}^2+k_\mathrm{ty}^2}$ represent their wave vectors, which can be decomposed along the x and y directions. Substituting Eq. (2) and relative parameters into Eq. (1), we will obtain the electromagnetic field solution for the air and LN crystal regions including H_ix, H_iy, H_rx, H_ry, H_tx, H_ty for incident wave, reflection wave, and transmission wave respectively. Subsequently, the reflection coefficient and transmission coefficient of the incident wave can be obtained by adopting the standard continuous boundary conditions of the electromagnetic tangential components, and the answer is

$$\begin{aligned}r&=\frac{E_\mathrm{rz}}{E_\mathrm{iz}}=\frac{\cos\alpha-\sqrt{n_1^2-\sin^2\alpha}}{\cos\alpha+\sqrt{n_1^2-\sin^2\alpha}},\\ t&=\frac{E_\mathrm{tz}}{E_\mathrm{iz}}=\frac{2\cos\alpha}{\cos\alpha+\sqrt{n_1^2-\sin^2\alpha}}.\end{aligned}\tag{3}$$

We also analyze the energy flux of wave by calculating the average Poynting vector $\boldsymbol{S}=\frac{1}{2}\mathrm{Re}\,(\boldsymbol{E}\times\boldsymbol{H})$. After further simplification, the reflectance and transmittance in regard to energy power of FW light are obtained as follows:

$$R=\left(\frac{\cos\alpha-\sqrt{n_1^2-\sin^2\alpha}}{\cos\alpha+\sqrt{n_1^2-\sin^2\alpha}}\right)^2,$$

$$T=\frac{4\cos\alpha\sqrt{n_1^2-\sin^2\alpha}}{\left(\cos\alpha+\sqrt{n_1^2-\sin^2\alpha}\right)^2}.\tag{4}$$

2.2. Obliqueincidence nonlinear coupled wave theory for FW and SHW

In the reflection and transmission model of the air-crystal interface, we consider two nonlinear conversion processes simultaneously, including FW exciting SHW ($\omega_1+\omega_1=\omega_2$) and SHW coupling with FW ($\omega_2-\omega_1=\omega_1$) in LN crystal. Since the wave equations are used to describe the propagation and interaction of light waves in a general medium, we derive the nonlinear coupled-wave equations starting from the wave equations, which can be written as

$$\nabla^2E_1-\mu_0\varepsilon_0\varepsilon_1\frac{\partial^2E_1}{\partial t^2}=\mu_0\frac{\partial^2P_\mathrm{NL}(\omega_1)}{\partial t^2},\tag{5}$$

$$\nabla^2E_2-\mu_0\varepsilon_0\varepsilon_2\frac{\partial^2E_2}{\partial t^2}=\mu_0\frac{\partial^2P_\mathrm{NL}(\omega_2)}{\partial t^2},\tag{6}$$

where $P_\mathrm{NL}(\omega_1)$ and $P_\mathrm{NL}(\omega_2)$ are second-order nonlinear polarizations, and they are new radiation sources of FW and SHW in LN crystal. E_1 and E_2 represent the electric fields for monochromatic wave at the angular frequency ω_1 of FW and ω_2 of SHW in crystal. Note that these two electric fields have only the z-component polarization, so we can obtain the scalar $P_\mathrm{NL}(\omega_1)$, $P_\mathrm{NL}(\omega_2)$ from the nonlinear polarization $\boldsymbol{P}_\mathrm{NL}(\omega_2)=\boldsymbol{P}^{(2)}(\omega_2)\,\mathrm{e}^{-\mathrm{i}\omega_2 t}=\widehat{z}\varepsilon_0\chi^{(2)}E_1E_1$ and $\boldsymbol{P}_\mathrm{NL}(\omega_1)=\boldsymbol{P}^{(2)}(\omega_1)\,\mathrm{e}^{-\mathrm{i}\omega_1 t}=\widehat{z}2\varepsilon_0\chi^{(2)}E_2E_1^*$, where the second-order nonlinear susceptibility tensor is $\chi^{(2)}=2d_{33}$ for the general LN crystal. Further, the wave functions for the transmitted FW and SHW are supposed to be

$$E_1=E_{10}\,\mathrm{e}^{-\mathrm{i}k_{1x}x+\mathrm{i}k_{1y}y}\,\mathrm{e}^{-\mathrm{i}\omega_1 t},\tag{7}$$

$$E_2=E_{20}\,\mathrm{e}^{-\mathrm{i}k_{2x}x+\mathrm{i}k_{2y}y}\,\mathrm{e}^{-\mathrm{i}\omega_2 t},\tag{8}$$

where E_{10}, E_{20} are the electric field amplitudes of FW and SHW, assumed to be varying slowly along the y direction. k_{1x}, k_{2x}, k_{1y}, and k_{2y} denote the components of transmission FW vector k_1 and SHW vector k_2 in the x and y directions, which satisfy $k_1^2=k_{1x}^2+k_{1y}^2$ and $k_2^2=k_{2x}^2+k_{2y}^2$. Thus we have $k_{1x}=k_1\sin\beta=(\omega_1/c)n_1\sin\beta$ and $k_{2x}=k_2\sin\gamma=(\omega_2/c)n_2\sin\gamma$. Considering the photon momentum conservation between incident FW light, transmitted FW light, and generated SHW light in the x direction, we find $2k_{1x}=k_{2x}=2k_\mathrm{ix}=2(\omega_1/c)\sin\alpha$ and the phase mismatching in x direction can be written as

$$\Delta k_x=2k_{1x}-k_{2x}=0.\tag{9}$$

Then, the phase mismatching between FW and SHW exists only in the y direction, which can be given by

$$\Delta k_y=2k_{1y}-k_{2y}.\tag{10}$$

By substituting E_1, E_2, $P_{\rm NL}(\omega_1)$, $P_{\rm NL}(\omega_2)$, Δk_x, Δk_y into Eqs. (5) and (6), we eventually derive the coupled-wave equations for SHG in a general LN crystal in the case of the slowly-varying amplitude approximation, which can be expressed in the following form:

$$\frac{\partial E_{10}}{\partial y} = \frac{2\mathrm{i}\mu_0\varepsilon_0 d_{33}\omega_1^2}{k_{1y}} E_{10}^* E_{20}\,\mathrm{e}^{-\mathrm{i}\Delta k_y y}, \tag{11}$$

$$\frac{\partial E_{20}}{\partial y} = \frac{\mathrm{i}\mu_0\varepsilon_0 d_{33}\omega_2^2}{k_{2y}} E_{10}^2\,\mathrm{e}^{\mathrm{i}\Delta k_y y}. \tag{12}$$

After solving Eqs. (11) and (12), the electric fields at any position within the LN crystal can be obtained. Here, $y = L_{\rm eff} = L\cos\beta$ represents the effective transporting distance of light within the crystal in the y direction, but L is the actual distance the FW propagates. As a result, the phase mismatching of the LN crystal in the y direction can be calculated as

$$\Delta k_y = \frac{4\pi}{\lambda_1}\left[\sqrt{n_1^2 - \sin^2\alpha} - \sqrt{n_2^2 - \sin^2\alpha}\right]. \tag{13}$$

For convenience, we refer to Δk_y as the oblique-incidence phase mismatching, which closely relies on the incident angle α and the pump wavelength λ_1.

When the pump light strikes the nonlinear crystal with different incident angles, it can be noticed obviously that the propagation of FW and SHW wave vectors k_1, k_2 are non-collinear, due to the unequal angles β and γ caused by the dispersion $n_1 \neq n_2$ of the LN crystal. Spontaneously, the transmission of FW and generated SHW will encounter a walk-off effect. We define the walk-off distance from FW and SHW in the x direction as walk-off length $\Delta x = |x_{\rm FW} - x_{\rm SHW}|$. Here, $x_{\rm FW} = y\tan\beta$ and $x_{\rm SHW} = y\tan\gamma$ are the tangential position of FW and SHW light beam at the crystal length of y, corresponding to different incident angle α. The walk-off length can be expressed by

$$\Delta x = \left| y\left(\frac{\sin\alpha}{\sqrt{n_2^2 - \sin^2\alpha}} - \frac{\sin\alpha}{\sqrt{n_1^2 - \sin^2\alpha}}\right)\right|. \tag{14}$$

According to Eq. (14), it can be intuitively observed that the walk-off length Δx is intrinsically controlled by the incident angle, the pump wavelength and the crystal length. After a simple calculation, we find that the walk-off length changes with incident angle and incident wavelength.

2.3. Rigorous solutions of oblique-incidence coupled wave equations in PPLN

The theoretical model described above for the reflection and transmission of pump light at the surface of an LN crystal and the coupling theory are also applicable to a PPLN crystal. Due to the phase mismatching caused by the dispersion between FW and SHW in general LN crystals, the PPLN crystal can effectively solve this problem with its own lattice structure via the QPM technique. Here, we select a PPLN crystal with first-order QPM structure to achieve a higher conversion efficiency. In this case, the PPLN crystal can provide an auxiliary reciprocal lattice vector (RLV) to compensate for the phase mismatching Δk_y, thus we can achieve the QPM condition $\Delta k_m = \Delta k_y - G_m = 0$, where $G_m = m(2\pi/\Lambda)$ is the m-th-order RLV provided by the PPLN crystal, Λ is the period length. The length of the positive and negative poling domains is both half of the poling period for the PPLN crystal, and the duty cycle D is 50%. In this case, we call χ_m ($\chi_m = 2\chi^{(2)}/\pi = 4d_{33}/\pi$) the effective second-order nonlinear polarization coefficient for first-order QPM.[16] Subsequently, the nonlinear coupled-wave equations (11) and (12) can be rewritten as

$$\frac{\partial E_{10}}{\partial y} = \frac{4\mathrm{i}\mu_0\varepsilon_0 d_{33}\omega_1^2}{\pi k_{1y}} E_{10}^* E_{20}, \tag{15}$$

$$\frac{\partial E_{20}}{\partial y} = \frac{8\mathrm{i}\mu_0\varepsilon_0 d_{33}\omega_1^2}{\pi k_{2y}} E_{10}^2. \tag{16}$$

Under the small signal approximation theory, the pump FW light is not depleted during the whole coupling process, and its intensity obeys $\partial E_{10}/\partial y = 0$ such that $E_{10} = $ constant. Additionally, the initial boundary conditions between FW and SHW are $E_{10}(y) = E_{10}(0)$, $E_{20}(0) = 0$, where the 0 or y in the bracket represent the chosen position in the y direction of PPLN crystal. Eventually, via solving Eq. (16), we can obtain the analytical expression of amplitude of SHW as

$$|E_2(y)|^2 = \frac{16 d_{33}^2\omega_1^2 y^2 t^4}{\pi^2 c^2\left(n_2^2 - \sin^2\alpha\right)}|E_{00}|^4, \tag{17}$$

where E_{00} represents the initial electric field amplitude of the incident pump wave. By means of calculating the average Poynting vector, we can get the relations between the field amplitude and field energy of incident wave, the transmission FW and the generated SHW in crystal. Then, we can derive the conversion efficiency of SHW in the form of

$$\eta = \frac{I_2(y)}{I_{00}} = \frac{32 n_2 d_{33}^2\omega_1^2 y^2 t^4 I_{00}}{\varepsilon_0 c^3\pi^2\left(n_2^2 - \sin^2\alpha\right)}, \tag{18}$$

where I_{00} is the initial intensity of the incident pump wave. In comparison to the case of small signal approximation, there is a consumption of FW energy under the general large signal theory. This means that the amplitude of the pump wave is a variant, varying with the propagation distance, and thus $\partial E_{10}/\partial y \neq 0$. Combining the initial boundary conditions of $E_{10}(0) = E_{00} \neq 0$ and $E_{20}(0) = 0$, we further solve both the nonlinear coupled-wave equations (15) and (16) to find rigorous solutions. Notice that, the 0 or y in the bracket represent the chosen position in the y direction of PPLN crystal. The analytical expressions of field amplitude for FW and SHW can be derived as

$$|E_{10}(y)|^2 = t^2 |E_{00}|^2 \operatorname{sech}^2 \left(\frac{\omega_1 t}{c\sqrt{n_2^2 - \sin^2\alpha}} \frac{4d_{33}}{\pi} \left[\frac{\sqrt{n_2^2 - \sin^2\alpha}}{\sqrt{n_1^2 - \sin^2\alpha}} \right]^{1/2} |E_{00}| y \right), \tag{19}$$

$$|E_{20}(y)|^2 = \frac{\sqrt{n_1^2 - \sin^2\alpha}}{\sqrt{n_2^2 - \sin^2\alpha}} t^2 |E_{00}|^2 \tanh^2 \left(\frac{\omega_1 t}{c\sqrt{n_2^2 - \sin^2\alpha}} \frac{4d_{33}}{\pi} \left[\frac{\sqrt{n_2^2 - \sin^2\alpha}}{\sqrt{n_1^2 - \sin^2\alpha}} \right]^{1/2} |E_{00}| y \right). \tag{20}$$

Ultimately, the conversion efficiencies of FW and SHW at different incident angles when reflection and transmission are considered, can be explicitly calculated as

$$\eta_1 = \frac{I_1(y)}{I_{00}} = n_1 t^2 \operatorname{sech}^2 \left(\frac{\omega_1 t}{c\sqrt{n_2^2 - \sin^2\alpha}} \frac{4d_{33}}{\pi} \left[\frac{\sqrt{n_2^2 - \sin^2\alpha}}{\sqrt{n_1^2 - \sin^2\alpha}} \right]^{1/2} |E_{00}| y \right), \tag{21}$$

$$\eta_2 = \frac{I_2(y)}{I_{00}} = \frac{\sqrt{n_1^2 - \sin^2\alpha}}{\sqrt{n_2^2 - \sin^2\alpha}} n_2 t^2 \tanh^2 \left(\frac{\omega_1 t}{c\sqrt{n_2^2 - \sin^2\alpha}} \frac{4d_{33}}{\pi} \left[\frac{\sqrt{n_2^2 - \sin^2\alpha}}{\sqrt{n_1^2 - \sin^2\alpha}} \right]^{1/2} |E_{00}| y \right). \tag{22}$$

It can be clearly seen that the conversion efficiencies of FW and SHW are closely related to the transmission coefficient t (as seen in Eq. (3)). Besides, the crystal length, the nonlinear polarization tensor, the wavelength of incident light as well as the field amplitude of pump wave are several key factors that determine the conversion efficiencies of FW and SHW.

Up to now, the nonlinear coupled-wave equations have been established for the pump light incident upon the crystal at different angles and fully considering the reflection and transmission of the interface, and the corresponding SHG conversion efficiencies of a PPLN crystal have been delicately solved under the large and small signal theories. All the details of electromagnetic wave transport properties and nonlinear conversion can be demonstrated and solved. Based on the analytical solution, we can evaluate not only qualitatively but also quantitatively the transmission behavior and tunable characteristics of the SHG process in a PPLN crystal at the QPM interaction under the oblique-incidence pump configuration of laser architecture.

3. Simulation results

3.1. Reflection and transmission of interface

In order to visualize the effect of reflection and transmission at the LN and PPLN crystal interface, we assume that the specific wavelength of incident pump light is 1064 nm, and calculate the corresponding refractive index of FW by Sellmeier formula.[40] Here, the influence of incident angle on reflection and transmission (r, t, R, T) is explored according to Eqs. (3) and (4), and the results are clearly illustrated in Fig. 2.

It can be seen from Fig. 2(a) that the reflection coefficient of the incident light increases with the incident angle from 0° to 90° while the transmission coefficient decreases with the increasing incident angle. As adequately described in Fig. 2(b), when the angle of incidence gets larger, the reflectivity of light energy also increases but the transmittance falls down monotonously. These phenomena are consistent with the rule that the more light is reflected, the less light is transmitted, and *vice versa*.

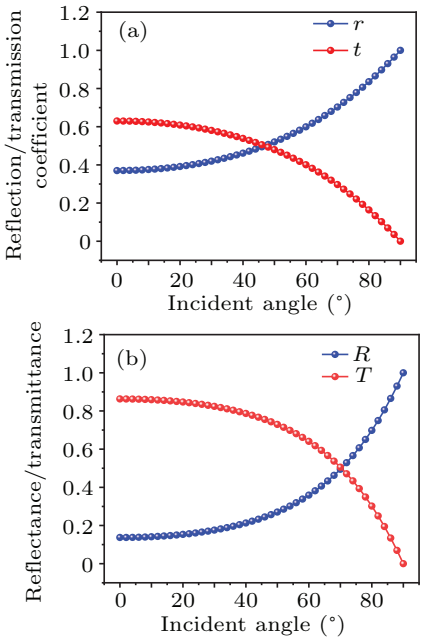


Fig. 2. (a) Field and (b) energy reflection and transmission for FW plane wave laser beam incident from air to LN and PPLN crystal at various oblique angles α.

3.2. Walk-off effect of FW and SHW

In accordance with Eq. (14), the walk-off length Δx is intrinsically controlled by the incident angle and incident wavelength, besides the crystal length. At a fixed incident pump wavelength of 1064 nm, together with the length of LN and PPLN crystal is $y = 10$ mm, the tendency of walk-off length Δx in dependence on the incident angle α is calculated and plotted in Fig. 3(a). Further, we investigate the trend of walk-off length Δx with respect to incident wavelength at a fixed

incident angle of 30° for a 10-mm-length LN and PPLN crystal in Fig. 3(b).

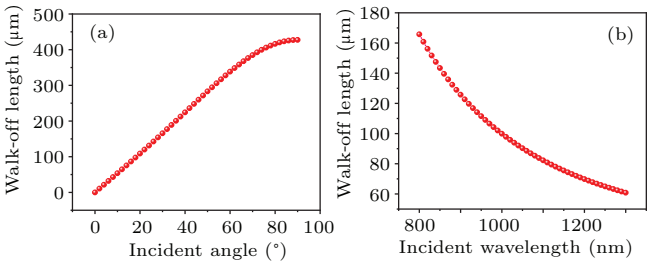


Fig. 3. The walk-off length of FW and SHW beams as a function of (a) incident angle at the wavelength of 1064 nm and (b) pump wavelength at the incident angle of 30° in LN and PPLN crystals.

As can be seen from Fig. 3(a), the larger incident angle makes the FW and SHW transmit in two different routes separately, which easily causes the walk-off in the x direction. Moreover, as the incident wavelength turns longer, the walk-off length will get shorter for a specific incident angle. It can be concluded that, a suitable incident wavelength or incident angle can suppress the walk-off effect to some extent. For efficient nonlinear coupling, we prefer to get a slight walk-off effect by choosing a smaller incident angle or a longer incident wavelength.

3.3. Matched wavelength of incident pump laser

In accordance with phase mismatching formula, as shown in Eq. (13), it can be accurately calculated that the phase mismatching is $|\Delta k_y| = 0.901\ \mu\text{m}^{-1}$, in the situation where the incident pump light wavelength is 1064 nm and the incident angle is 0°. The m-th-order RLV G_m of the single specific PPLN sample used in our numerical simulations is represented as $G_m = m(2\pi/\Lambda) = \Delta k_y$, which compensates for the value of phase mismatching via QPM technique. For such a fixed phase mismatching Δk_y for an identified PPLN sample, we can investigate the phase matching wavelength of incident pump light λ_1 varying with the incident angle α, and the result is displayed in Fig. 4.

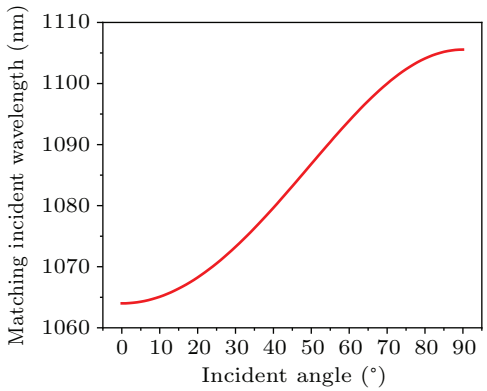


Fig. 4. The phase matching wavelength of pump light as a function of incident angle for phase mismatching $|\Delta k_y| = 0.901\ \mu\text{m}^{-1}$ at the wavelength of 1064 nm between transmission FW and generated SHW in crystal.

Note that there is a specific matching incident wavelength at a specific angle of incidence, which corresponds one by one. Further analysis, we can find that the phase matching wavelength of pump light increases monotonically when the incident angle becomes larger. What needs illustration is that in most experimental cases, the Brewster angle is the first choice, which is mainly to minimize the reflected light energy and maximize the transmitted light energy, so as to improve the conversion efficiency of related experiments. However, in our model, we are mainly concerned with the extent to which a tunable spectrum bandwidth range can be achieved by introducing the 0° to 90° of incident angle engineering, which shows a trend of monotonic increasing. Besides, the conversion efficiency of the SHW gradually decreases with the increasing incident angle. That is to say, a compromise between the high conversion efficiency and tunable narrow-band bandwidths is fully taken into account in our scheme, rather than preferring the angle of least reflection. Under this scheme, if the range of incident angles can be idealized from 0° to 90° the phase matching wavelength of the FW can tune in the range of 1064 nm–1105.6 nm, with a rather large bandwidth of about 41.6 nm, which obviously is much larger than in the usual way of temperature or period fine tuning. According to our theoretical calculations, when the temperature of the PPLN crystal rises from 20 °C–200 °C by temperature tuning and the pump light stays at 0° incident on the crystal, the FW tuning range is 1063.66 nm to 1081.03 nm with a tuning range of 17.37 nm. The tuning range of this method is more limited than the angle tuning method proposed in our study. In addition, there are several problems with temperature tuning, including the requirement for high-precision temperature control equipment, the effect of temperature drift on wavelength stability, and the long response time of high-low temperature switching, and the crystal life is easy to degrade at high temperature. Indeed, it has been reported earlier that the output wavelength can be tunable by designing a single PPLN crystal with a fan structure, or by cascading multiple crystals to form different periodic structures, but with a complicated experimental setup and low conversion efficiency. In contrast, our method provides a new degree of freedom for efficient and tunable narrow-band second harmonic generation by introducing single incident angle modulation in PPLN crystals. In other words, one can simply adjust and match the incident angle corresponding to a given incident wavelength for the output the different wavelengths of SHW, and this would effectively break the limitation that a single PPLN crystal can only achieve a specific wavelength matching. Thus, it is possible to realize the nonlinear process of generating tunable narrow-band wavelength output for a single PPLN crystal based on angle-engineering.

3.4. RLVs distributions and dispersion curves

As has been pointed out, a single PPLN crystal can match different wavelengths of incident FW by choosing the corresponding appropriate incident angle. Here, the sample we use is a z-cut PPLN crystal with the dimensions of 5 mm

$(x)\times 10$ mm $(y)\times 1$ mm (z). The poling period of the PPLN crystal $\Lambda = 6.974$ μm is given by $\Lambda = 6.974$ μm $(m = -1)$, and the duty ratio is 1:1. Distribution of RLVs and the phase mismatching dispersion curves at incident angle 0°, 20°, 40°, and 60° in PPLN crystal with QPM structure are calculated and plotted in Fig. 5.

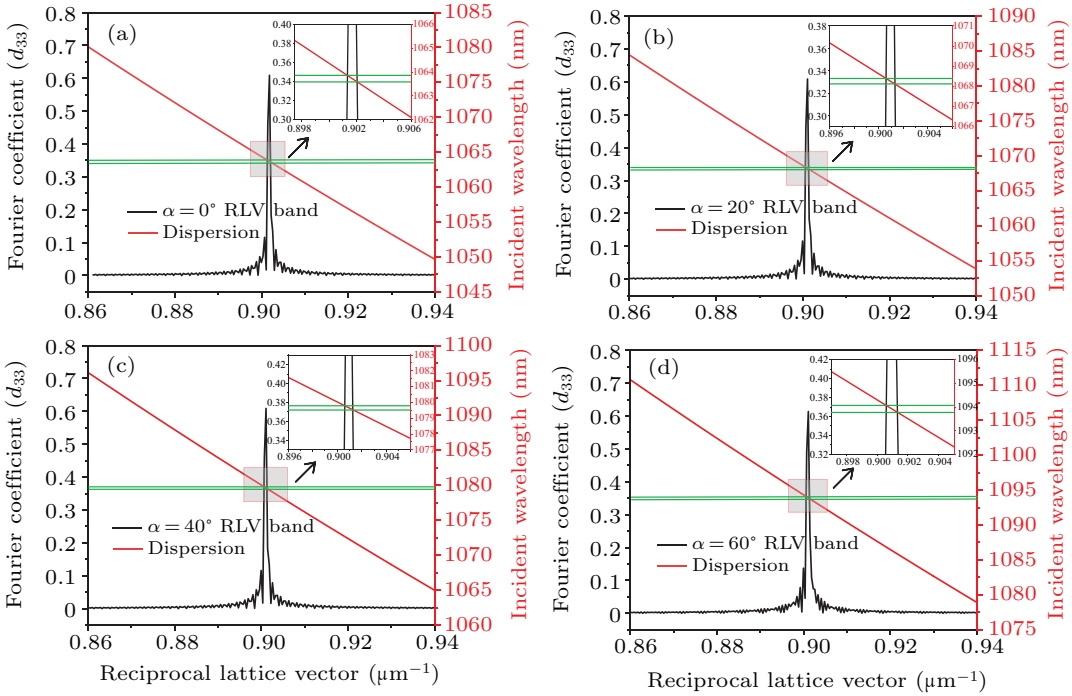


Fig. 5. Distribution of RLVs and the phase mismatching dispersion curves at incident angle (a) 0°, (b) 20°, (c) 40°, and (d) 60°, respectively in PPLN crystal with first order QPM structure.

As shown in Fig. 5(a), when the incident angle is $\alpha = 0°$, the RLV provided by PPLN crystal presents a sharp peak, and the peak value is with high Fourier coefficient of $(2/\pi)d_{33}$. What is more, the phase mismatching dispersion curve intersects the RLV peak right at 0.901 μm^{-1}, which exactly matches the central wavelength of 1064 nm. It means that the designed PPLN crystal can compensates the specific phase mismatching $|\Delta k_y| = 0.901$ μm^{-1} between FW and SHW when SHG occurs at the incident wavelength of 1064 nm. For easy comparison, when the incident angles are 20°, 40°, and 60°, respectively, and the results are depicted in Figs. 5(b)–5(d). Evidently, for a specific PPLN crystal, the incident wavelength for phase matching will change when the pump light is incident at different angles, so as to achieve QPM. In more detail, the intersection of the RLV and the phase mismatching dispersion curve occurs at the pump wavelengths of 1064 nm, 1068.3 nm, 1079.7 nm, and 1093.9 nm at incident angles of 0°, 20°, 40°, and 60°, respectively. Meanwhile, the peak of the RLVs remains at $|\Delta k_y| = 0.901$ μm^{-1}, and the matching wavelength of pump light turns longer when the incident angle is larger. One thing worth noting is that, the actual incident angle cannot be set to 90° because the PPLN crystal does not have a corresponding domain structure along x direction. Therefore, when the incident angle changes from 0° to 90° the PPLN crystal with first order QPM design is appropriate for phase-mismatching compensation at incident wavelength 1064 nm–1105.6 nm, which corresponds to the output SHW of 532 nm–552.8 nm, with a considerable tunable bandwidth of 20.8 nm. This marks the realization of narrow-band tunability for the SHW in an angle-engineered PPLN crystal by means of regulating the incident angle in match with the pump wavelength.

3.5. SHW conversion efficiency

Finally, we fully consider the reflection and transmission at the crystal surface and discuss how the incident wavelength modulates the SHW conversion efficiency under general large signal theory. Similarly, we continue to analyze the incident angle of 0°, 20°, 40°, and 60°. The amplitude of the incident wave is $E_{00} = 6 \times 10^6$ V/m, which has great influence on the conversion efficiency. At the same time, the results in Fig. 6, based on our model, also depend on the various parameters given by the analytic Eqs. (21) and (22) we derived, including the electric field amplitude, the crystal length, the incident angle, etc. Under the reflection and transmission model, the conversion efficiency of SHW is a function of phase matching wavelength of pump light at different incident angles, as displayed in Fig. 6. This is based on the lattice inverse vector obtained from the Fourier transform of the crystal domain structure in Fig. 5 to further calculate the conversion efficiency in the corresponding matching wavelength range, which is a reasonable explanation for why our final numerical simulation result is not a symmetric Gaussian distribution.

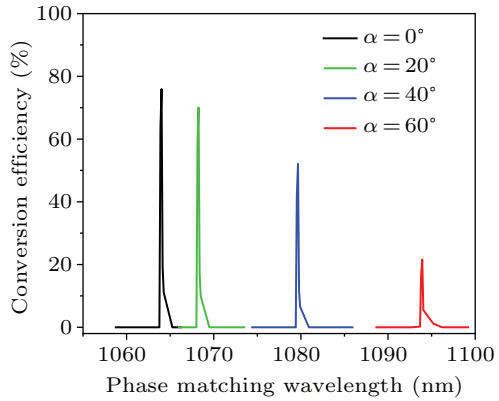


Fig. 6. The conversion efficiency of SHW as a function of phase matching wavelength of the FW when the incident angles is 0° (black line), 20° (green line), 40° (blue line), 60° (red line), respectively.

From Fig. 6, SHG efficiency decreases obviously as the incident angle gets larger at a certain incident wavelength. When the pump light is incident at angles 0°, 20°, 40°, and 60° the incident wavelengths of 1064.0 nm, 1068.3 nm, 1079.7 nm, and 1093.9 nm can be chosen to reach a maximum SHG efficiency about 75.9%, 70.1%, 52.1%, and 21.6%, respectively. These results can be explained from two aspects. Firstly, as the incident angle increases, the amplitude of the electric field (E_{10}) entering the PPLN crystal will gradually decrease under the consideration of interface transmission. For $\alpha = 0°$, the field amplitude of FW transmitted into the crystal is 3.81×10^6 V/m, and it drops sharply to 1×10^6 V/m when the incident angle α increases to 80°. On the other hand, with the increased incident angle, the interaction length of FW in the crystal becomes significantly shorter, which reduces the conversion efficiency of SHW to some extent. Under the condition that other conditions remain unchanged, we also can try to increase the anti-reflection film plating at the outlet end to increase the light output energy, so as to further improve the conversion efficiency at a large angle. It demonstrates that for a certain incident angle, we can find a specific incident wavelength to get a maximum SHG efficiency, i.e., the optimum phase matching incident wavelength or optimum phase matching incident angle. Thus, we can ideally extend the incident angles from 0° to 90° and get narrow-band tunability of the incident wavelengths from 1064 nm to 1105.6 nm in the particular PPLN crystal through QPM schemes, resulting in narrow-band tunable SHW output.

4. Conclusions

In summary, we have proposed an angle-engineering QPM scheme and shown that the incident angle of pump laser light can be harnessed as an alternative versatile tool to engineer QPM for high-efficiency SHG in a PPLN crystal, in addition to conventional means of period adjusting or temperature tuning. We have provided a nonlinear optical theoretical system to investigate nonlinear SHG process in PPLN crystal under different incident angles of pump light. First, we have established the formalism of nonlinear coupled wave equations for SHG suitable for oblique incidence, fully considering the reflection and transmission of FW pump light at air-crystal surface. Second, under both the small signal approximation model and the general large signal model, we have rigorously solved the coupled-wave equations and derived the explicit analytical expressions of SHW field intensity and the SHG conversion efficiency for both artificial LN crystal and PPLN crystal. For a PPLN crystal, a well-established effective nonlinear coefficient model has been adopted. Finally, we have systematically analyzed the walk-off effect and the phase mismatching of FW and SHW in dependence on incident angle or pump wavelength within LN crystal and PPLN crystal.

We have performed systematic numerical simulations for a PPLN crystal with first order QPM structure to confirm our theoretical predictions for several interesting phenomena based on the exact analytical solution of the general large-signal theory. We have determined the one-to-one correspondence between the pump incident light wavelengths and the phase matching incident angle of pump light. The results show that the narrow-band tunable SHG output covers a range of 532 nm–552.8 nm at the ideal incident angles from 0° to 90°. Yet, this bandwidth has already been much larger than in the usual way of temperature or period phase matching tuning, which is on the order of 1 nm. Besides, the conversion efficiency of the SHW gradually decreases with the increasing incident angle, and this might be improved by anti-reflection coating on the LN crystal surface.

The proposed angle-engineering scheme has offered an alternative route to realize tunable QPM with a considerable broad bandwidth for high-efficiency SHG against pump laser for a pre-designated PPLN crystal, and this scheme has a superior performance compared with conventional means of period adjusting or temperature tuning in terms of tunability bandwidth. Moreover, the developed analytical theory and formalism, which fully consider the reflection and transmission at the air-crystal interface, would offer an efficient theoretical system to evaluate quantitatively the nonlinear frequency conversion processes and help to obtain the maximum SHG conversion efficiency by selecting an optimum incident wavelength and incident angle in a specially designed PPLN crystal. The angle-engineering QPM scheme and associate analytical formalisms can be readily extended to handle other nonlinear optical processes such as SFG and DFG. Together they would be very helpful for the design of tunable narrow-band pulse nanosecond, picosecond, and femtosecond laser devices via PPLN and other microstructured LN crystals.

Acknowledgements

Project supported by the National Natural Science Foundation of China (Grant No. 11974119), the Science and Technology Project of Guangdong Province, China

(Grant No. 2020B010190001), the Guangdong Innovative and Entrepreneurial Research Team Program (Grant No. 2016ZT06C594), the National Key Research and Development Program of China (Grant Nos. 2018YFA, 0306200, and 2019YFB2203500), and the Science and Technology Program of Guangzhou City (Grant No. 2023A04J1309).

References

[1] Maiman T H 1960 *Nature* **187** 493
[2] Chen B Q, Zhang C, Liu R J and Li Z Y 2014 *Appl. Phys. Lett.* **105** 151106
[3] Zhang J, Huang J Y, Wang H, Wong K S and Wong G K 1998 *JOSA B* **15** 200
[4] Zhu S N, Zhu Y Y, Qin Y Q, Wang H F, Ge C Z and Ming N B 1997 *Phys. Rev. Lett.* **78** 2752
[5] Yang F, Wang Z, Zhou Y, Li F, Xu J, Xu Y, Cheng X, Lu Y, Bo Y, Peng Q, Cui D, Zhang X, Wang X, Zhu Y and Xu Z 2009 *Appl. Phys. B* **96** 415
[6] Broderick N G R, Ross G W, Offerhaus H L, Richardson D J and Hanna D C 2000 *Phys. Rev. Lett.* **84** 4345
[7] Franken P A and Ward J F 1963 *Rev. Mod. Phys.* **35** 23
[8] Herman W N and Hayden L M 1995 *JOSA B* **12** 416
[9] Ni P, Ma B, Wang X, Cheng B and Zhang D 2003 *Appl. Phys. Lett.* **82** 4230
[10] Berger V 1998 *Phys. Rev. Lett.* **81** 4136
[11] Yan S, Dou J, Ma B, Cheng B and Zhang D 2007 *Appl. Phys. Lett.* **91** 011101
[12] Fejer M M, Magel G A, Jundt D H and Byer R L 1992 *IEEE J. Quantum Electron.* **28** 2631
[13] Ma B Q, Wang T, Sheng Y, Ni P G and Wang Y Q 2005 *Appl. Phys. Lett.* **87** 251103
[14] Zhao L M, Yue G K, Zhou Y S and Wang F H 2013 *Opt. Express* **21** 17592
[15] Ren M L and Li Z Y 2010 *Opt. Express* **18** 7288
[16] Ren M L and Li Z Y 2011 *Europhys. Lett.* **94** 44003
[17] Nikogosyan D N 2006 *Nonlinear optical crystals: a complete survey* (Springer Science & Business Media)
[18] Arizmendi L 2004 *Phys. Status Solidi* **201** 253
[19] Armstrong J A, Bloembergen N, Ducuing J and Pershan P S 1962 *Phys. Rev.* **127** 1918
[20] Chen B Q, Ren M L, Liu R J, Zhang C, Sheng Y, Ma B Q and Li Z Y 2014 *Light Sci. Appl.* **3** e189
[21] Xu P, Ji S H, Zhu S N, Yu X Q, Sun J, Wang H T, He J L, Zhu Y Y and Ming N B 2004 *Phys. Rev. Lett.* **93** 133904
[22] McMullen J D 1975 *J. Appl. Phys.* **46** 3076
[23] Chen B Q, Zhang C, Hu C Y, Liu R J and Li Z Y 2015 *Phys. Rev. Lett.* **115** 083902
[24] Rustagi K, Mehendale S C and Meenakshi S 1982 *IEEE J. Quantum Electron.* **18** 1029
[25] Hu C Y and Li Z Y 2017 *J. Appl. Phys.* **121** 123110
[26] Lin J T, Bo F, Cheng Y and Xu J J 2020 *Photon. Res.* **8** 1910
[27] Boes A, Corcoran B, Chang L, Bowers J and Mitchell A 2018 *Laser Photon. Rev.* **12** 1700256
[28] Zhu D, Shao L B, Yu M J, Cheng R, Desiatov B, Xin C J, Hu Y W, Holzgrafe J, Ghosh S, Shams-Ansari A, Puma E, Sinclalr N, Reimer C, Zhang M and Lončar M 2021 *Adv. Opt. Photon.* **13** 242
[29] Vazimali M G and Fathpour S 2022 *Adv. Photon.* **4** 034001
[30] Poberaj G, Hu H, Sohler W and Günter P 2012 *Laser Photon. Rev.* **6** 488
[31] Born M and Wolf E 2013 *Principles of optics: electromagnetic theory of propagation, interference and diffraction of light* (Elsevier)
[32] Wang P Q 2018 *Appl. Opt.* **57** 4950
[33] McClain S C, Hillman L W and Chipman R A 1993 *JOSA A* **10** 2371
[34] Avendaño-Alejo M, Stavroudis O N and Goitia A R B Y 2002 *JOSA A* **19** 1688
[35] Avendaaño-Alejo M and Stavroudis O N 2002 *JOSA A* **19** 1674
[36] Liang Q T 1990 *Appl. Opt.* **29** 1008
[37] Mosteller L P and Wooten F 1968 *JOSA* **58** 511
[38] Simon M C 1983 *Appl. Opt.* **22** 354
[39] Lekner J 1991 *J. Phys.: Condens. Matter* **3** 6121
[40] Gayer O, Sacks Z, Galun E and Arie A 2008 *Appl. Phys. B* **91** 343